

Bonding and electronic structure in zirconia pseudopolymorphs investigated by electron energy-loss spectroscopy

David W. McComb*

Brockhouse Institute for Materials Research, McMaster University, Hamilton, Ontario, Canada L8S 4M1

(Received 5 March 1996)

The use of electron energy-loss spectroscopy for characterization of zirconium oxide pseudopolymorphs is investigated. The results demonstrate that spectroscopic “fingerprints” for each phase can be identified and the technique can be utilized for phase identification. The oxygen *K*-edge spectra are analyzed in detail and the spectral features are interpreted within the context of the electronic structure of zirconia. Comparisons between theory and experiment reveal coincidences which can result in misleading interpretations of the energy-loss and x-ray absorption spectra. It is shown that the effect of dopant atoms and oxygen vacancies in stabilized zirconias must be considered in order to derive the correct interpretation of the spectra. [S0163-1829(96)04233-6]

I. INTRODUCTION

Pressure tubes for CANDU reactors are made from Zr 2.5 wt. % Nb alloys by a process involving extrusion and cold drawing.^{1,2} Thin oxide films that form during stress-relieving steam treatments serve as barriers against hydrogen ingress. The oxide formed is primarily monoclinic ZrO₂, but the presence of low concentrations of tetragonal ZrO₂ may be important for comprehension of the growth mechanism. Owing to the small grain size, overlap between the grains, and structural ambiguities among the cubic (*c*), tetragonal (*t*), and monoclinic (*m*) phases, it is difficult to distinguish *t*-ZrO₂ and *c*-ZrO₂ in the presence of the *m*-ZrO₂ using diffraction methods.² Hydrogen ingress can have a detrimental influence on the mechanical properties and lifetime of the pressure tubes, yet the mechanism by which hydrogen diffuses through the oxide layer to the alloy is not well understood. It is important to obtain detailed information on the structural and electronic properties of the oxide layer, particularly in the vicinity of grain boundaries between different phases, to understand this process at the atomic level. Pure and stabilized zirconium oxides also have interesting ionic and mechanical properties that render them, useful in a variety of applications, including oxygen sensors, fuel cells and ceramic toughening agents.³ As a result of such wide-ranging applications, many investigations designed to correlate microstructure with properties have been carried out.⁴ Thus, in the current study, it is possible to draw upon a substantial body of crystallography and spectroscopy literature to aid development of the experimental method.

Using suitable model systems, the current work reports on the applicability of electron-energy-loss spectroscopy (EELS) carried out in the analytical electron microscope (AEM) as a characterization method. The high spatial resolution available in the AEM provides incentive to establish EELS characterization methods. The energy-loss spectrum exhibits “edges” due to the elements present in the specimen and quantification of such edges permits determination of the chemical composition. However, more pertinent to

this study is the energy-loss near-edge structure (ELNES), which is present at each edge and can be related to the local coordination environment.^{5,6} This study has two primary objectives; first, to determine if a “coordination fingerprint” exists in the energy-loss spectrum which can easily be utilized to distinguish among the zirconia pseudopolymorphs, and, second, to relate ELNES in each sample to the electronic structure and local coordination environment.

Monoclinic ZrO₂ can be described as a distorted fluorite structure with the Zr atoms in sevenfold coordination sites.^{7,8} There are two oxygen sites in the lattice; O1, where oxygen is coordinated to three Zr atoms in an almost planar environment, and O2, where the central atom is surrounded by a distorted tetrahedron of Zr atoms.⁷ The phase diagram shows that the tetragonal and cubic phases are stable only at high temperature.⁹ In the pure form, both of these phases contain ZrO₈ polyhedra and are based on the fluorite lattice.^{8,10} However, these phases can be stabilized at room temperature by the addition of suitable dopants, e.g. MgO, CaO, Y₂O₃, etc., to form tetragonal stabilized zirconia (TSZ) and cubic stabilized zirconia (CSZ) which are anion-deficient structures based on the fluorite unit cell. The effect of the extrinsic oxygen vacancies created by the dopants on the crystal structure of TSZ and CSZ has been investigated extensively using x-ray and neutron diffraction.^{11,12} Recent results suggest that oxygen atoms “relax” towards a vacancy producing a change in the local coordination around the zirconium atom.¹² Further, some evidence suggests that the O vacancies are preferentially located next to Zr atoms (rather than Y atoms) in Zr_{1-x}Y_xO_{2-0.5x} systems, and that such systems can therefore be modeled as a combination of YO₈, ZrO₈, and ZrO₇ polyhedra.¹³ The phase diagram shows that at low dopant concentration TSZ is the stable phase, while formation of CSZ requires higher concentrations.¹² Clearly, the number of O vacancies, and consequently the number of ZrO₇ polyhedra, is dependent on the dopant concentration. Thus, there is a continuous change in the average coordination number of zirconium, from about 8 in TSZ to nearly 7 in CSZ, as the dopant concentration is increased from a few percent to around 20%.

II. EXPERIMENTAL METHODS

Specimens of m -ZrO₂, TSZ, and CSZ were prepared for electron microscopy using conventional ion polishing techniques. The specimens were analyzed using energy-dispersive x-ray analysis in the electron microscope (JEOL-2010F) and the compositions measured were consistent with the supplier's¹⁴ specifications of 4.5M% (TSZ) and 9.5M% (CSZ) of Y₂O₃.

EELS was performed using a parallel recording system (Gatan 666) for which an optimum resolution of 0.55 eV has been attained. In this work, the energy resolution at the zero-loss peak was 0.6 eV for the valence losses and 0.9 eV for the core loss excitations. EELS was performed in scanning transmission mode with a convergence angle of approximately 6 mrad. The collection angle used varied depending on the excitation being investigated, being 5 mrad for low loss studies, 7 mrad for the Zr $M_{2,3}$ and O K edges and 12 mrad for the Zr $L_{2,3}$ edge. The spectra were acquired while scanning the electron probe over a uniformly thick area (142×117 nm²). The valence loss spectra, including the zero-loss peak, were collected after each core loss analysis using the same conditions, in order to deconvolute effects due to plural scattering.

The detector gain calibration and dark current were recorded and removed from each spectrum using the Gatan software routines. A sequence of eight (the maximum software permitted value) spectra was collected from each area, and the spectra within each sequence were aligned, then summed. A background of the form AE^{-r} was subtracted from summed core edges and the summed valence loss spectrum from the same area was used to remove contributions due to plural scattering. In the case of the Zr $M_{2,3}$ edge, the preceding $M_{4,5}$ edge makes background subtraction difficult. Thus, the deconvoluted and background-stripped M edge was obtained, then a straight-line extrapolation under the M_3 portion of the edge was used. Due to the limited energy range of the extrapolation, this is a reasonable approximation.

The effect of tailing, caused by the point spread function of the detector, was removed from the valence loss spectra using the ‘‘sharpen resolution’’ routine of the Gatan software. The resulting spectrum was smoothed using a 0.4 eV filter and a Fourier log deconvolution algorithm was employed to obtain the single-scattering distribution (SSD). The spectral intensity in the SSD was extrapolated to zero using a linear function. Kramers-Kronig analysis of the data was then performed to obtain the real (ϵ_1) and imaginary (ϵ_2) parts of the complex dielectric function. The dielectric function was normalized using the optical refractive index [$n=2.16$ for c -ZrO₂ (Ref. 15)].

III. VALENCE LOSS SPECTROSCOPY

The experimental valence loss spectra after deconvolution and subtraction of the zero-loss peak are shown in Fig. 1. There are many similarities among the three spectra in terms of the number of peaks and their energies. Peaks below 30 eV are primarily associated with collective excitations between the valence and conduction bands, while those above 30 eV can be identified as the zirconium $N_{2,3}$ edge.

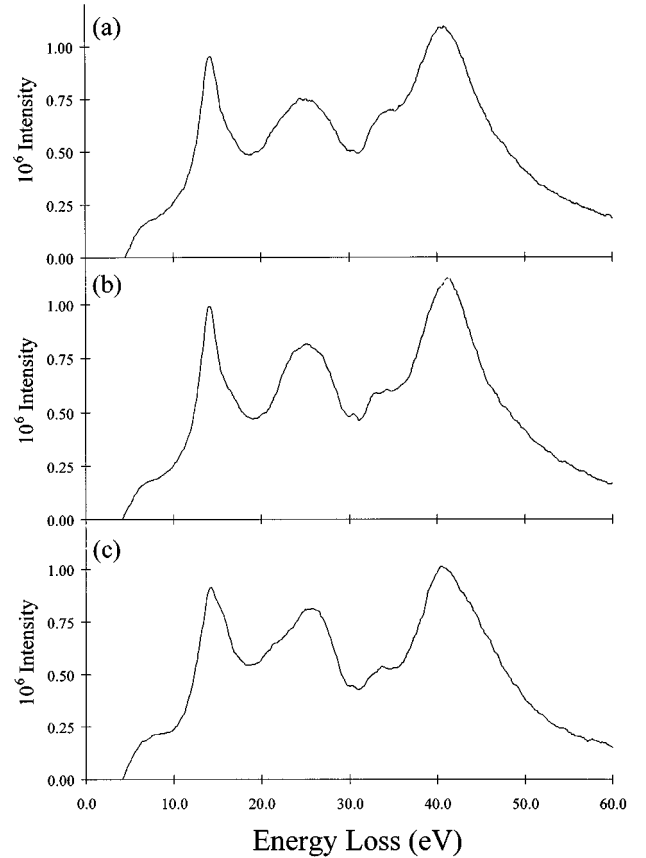


FIG. 1. Experimental valence loss spectra for (a) CSZ, (b) TSZ, and (c) m -ZrO₂.

The energy of the intensity threshold, within the error of the extrapolation described above, gives a reasonable measure of the size of the band gap, E_g . The values obtained from EELS data compare well with those obtained using other experimental methods, as well as those predicted theoretically (Table I). It is interesting to observe that same trend in the data from both EELS and VUV, although the VUV reflectance method tends to overestimate the magnitude of the band gap.¹⁶ In comparing experimental data with the calculations it should be noted that the majority of theoretical

TABLE I. Direct band-gap energy (eV) from experimental and theoretical methods.

	Monoclinic	Cubic	Tetragonal
EELS	4.2	4.6	4.2
(This work)			
Theor. (Ref. 16)	4.46	4.93	4.28
Theor. (Ref. 17)	7.1		
Theor. (Ref. 18)	4.51	3.84	4.11
Theor. (Ref. 19)		4.1	
Theor. (Ref. 20)		3.95	
Theor. (Ref. 21)		7.0	8.0
VUV (Ref. 16)	5.83	6.1	5.78
EELS (Ref. 22)	4.5		
VUV (Ref. 23)	4.5		
REELS (Ref. 24)	4.5		

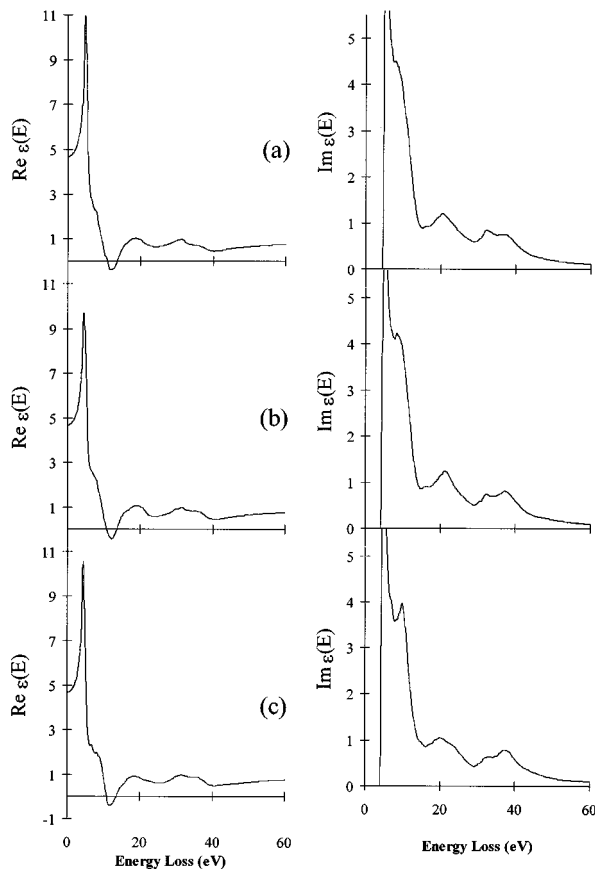


FIG. 2. Plots of the real (left) and imaginary (right) part of the complex dielectric functions for (a) CSZ, (b) TSZ, and (c) m -ZrO₂.

estimates are based upon an assumption of cubic symmetry without accounting for the effect of the stabilizing cations present in this phase at room temperature. The exceptions are the calculations due to Zandiehnam *et al.*¹⁸ and those due to French *et al.*¹⁶ where vacancy-free room-temperature structures for each phase were used.

All three phases show a broad unresolved peak in the low loss spectra at 8 eV which is due to excitation of valence electrons into the unoccupied d states in the conduction band.¹⁶ The sharp peak that occurs in the spectra at an energy of 14.2 eV may be interpreted as collective excitation of the bound electrons, i.e., a plasmon, since a zero of ϵ_1 is observed at this energy (Fig. 2). However, the oscillator strength or f sum-rule²⁵ plots shown in Fig. 3 reveal that the number of electrons involved in this plasmon excitation is around 5 per ZrO₂, a value considerably less than the 16 valence electrons per ZrO₂ unit expected based on $6e^-$ per oxygen atom ($2s^22p^4$) and $4e^-$ per zirconium ($4d^25s^2$). This discrepancy shows that the plasmon excitations are not exhausted at this energy, and in fact the broad maximum around 26 eV in all three spectra is associated in part with a collective excitation of all of the valence electrons. This assignment is confirmed by the observation of a minimum in ϵ_1 and small value of ϵ_2 (Fig. 2).

Differences in the imaginary part, ϵ_2 , of the dielectric functions (Fig. 2) of the three phases reflect dissimilarities in the joint density of states of the valence and conduction bands. These are more readily apparent in plots of the optical

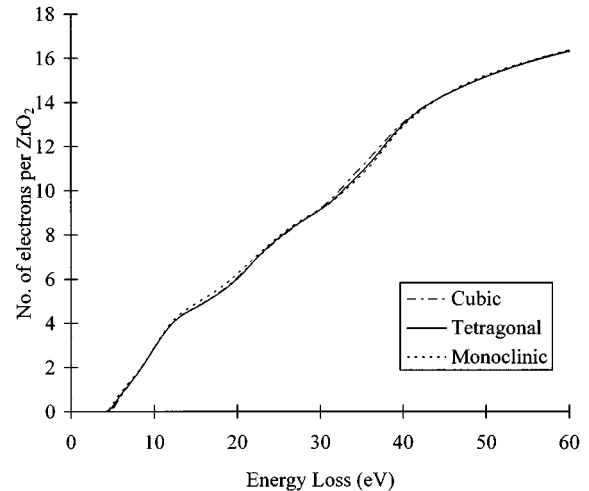


FIG. 3. Plot of the effective number of electrons, per formula unit, contributing to the valence loss spectrum of each pseudopolymorph of ZrO₂. There is essentially no difference among the three phases. The plateaus close to 14 and 26 eV correspond to the positions of the plasmon excitations in the valence loss spectra.

conductivity, $\sigma = i\omega\epsilon_2/4\pi$ (Fig. 4). For comparison, the plots of optical conductivity obtained by French *et al.*¹⁶ using reflectivity techniques are also shown. It should be noted that the energy, shape, and intensity of the first peak in ϵ_2 and σ are extremely sensitive to the extrapolation to zero intensity and for this reason little emphasis is placed on its interpretation. Other than in the vicinity of the fundamental gap, the agreement between the two techniques is reasonable. There appears to be a systematic discrepancy in the energy of the peaks at low-energy losses which requires further investigation. The transition energies from the energy-loss data are summarized in Table II using nomenclature consistent with that used by French *et al.*¹⁶ The lowest-energy transitions occur as a doublet centered around 7 eV (E_0) and are present only in m -ZrO₂. The first major peak (E_1) is at about 10 eV in all three phases. This peak is sharpest for m -ZrO₂, and exhibits a shoulder on the high-energy side in both the monoclinic and CSZ phases. In CSZ, the E_1 peak contains extensive fine structure, while in the TSZ phase it appears to be a broad, unresolved band. A small shoulder (E_2) is present at 16.0 eV in both the cubic and tetragonal phases. It was suggested by French *et al.*¹⁶ that this band could be associated with the stabilizing cations, which may be consistent with the fact that the band is at significantly lower energy, 15.2 eV, in the monoclinic phase. In contrast to the E_1 band, the E_3 peak at around 21 eV is broadest in m -ZrO₂, and is again characterized by a number of transitions up to about 23 eV.

The onset of a major transition, which may be identified as the zirconium $N_{2,3}$ edge, is observed at 29 eV. The $N_{2,3}$ edges are shown in more detail in Fig. 5. The three spectra all exhibit similar characteristics, namely a small prepeak near the threshold followed by a broader peak at around 34 eV and a strong excitation centered near 41 eV. Care must be taken in interpreting the fine structure of this edge since some of the features could be associated with valence-to-conduction-band transitions originating from the oxygen $2s$ valence level. It is tempting to assign the prepeak as being

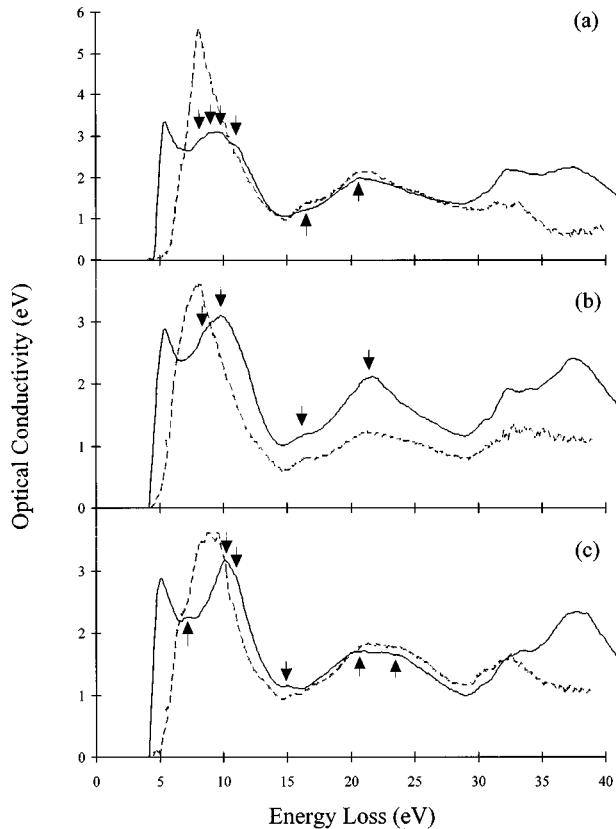


FIG. 4. Plots of the optical conductivity of (a) CSZ, (b) TSZ, and (c) m -ZrO₂ as calculated from the valence loss spectra. The arrows mark the major features as listed in Table II. Shown for comparison as broken lines are the optical conductivity plots obtained by French *et al.* (Ref. 16).

due to transitions to defect states introduced by the stabilizing cations, but as it is present in all three spectra this is not the case. There are subtle differences between the spectra, particularly in the number of peaks around 34 eV, as well as in the energy of the main peak, which is close to 41 eV. Clearly, there is an energy shift of this peak among the three phases and since the presence of the zero-loss peak permits precise determination of its energy, this peak could be used to distinguish among the three phases.

TABLE II. Transition energies (eV) determined from electron-energy-loss spectroscopy.

	Cubic	Tetragonal	Monoclinic
E_0			6.9,7.2
$E_{1'}$	8.0	8.4	
E_1	8.8,9.6	9.8	10.1
$E_{1''}$	11.2		10.9
E_2	16.0	16.0	15.2
E_3	20.7	21.7	20.1
$E_{3''}$			22.4

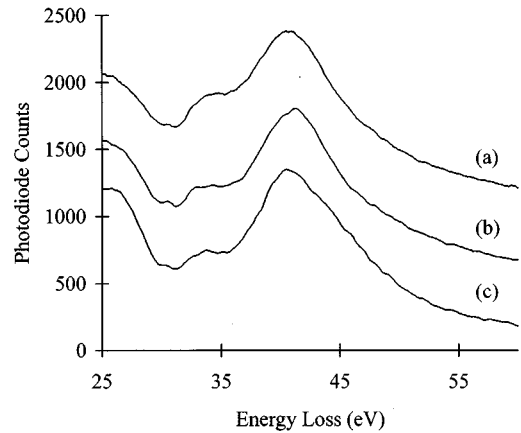


FIG. 5. Zirconium $N_{2,3}$ edges for (a) CSZ, (b) TSZ, and (c) m -ZrO₂.

IV. CORE LOSS SPECTROSCOPY

A. Core loss “fingerprints”

The Zr $L_{2,3}$ edge has been used in x-ray-absorption spectroscopy (XAS) studies to investigate the influence of Zr as an impurity in Y₂O₃.^{17,26} The edge consists of two narrow, intense lines which are generated by transitions from the metal $2p_{1/2}(L_2)$ and $2p_{3/2}(L_3)$ core levels to conduction-band states formed primarily from the unoccupied metal d orbitals. It is well established that these so-called “white” lines will exhibit a further splitting owing to the influence of the ligand-field on the d orbitals, and this has been extensively studied in the $3d$ transition-metal oxides.^{27–29} XAS studies have shown that the Zr L_2 edge exhibits this type of splitting in m -ZrO₂ with a magnitude of 2.1 eV.¹⁷ The Zr $L_{2,3}$ edge in all three pseudopolymorphs was investigated using EELS. While the energy-loss spectra obtained suggest that the white lines are comprised of at least two contributions, it proved difficult to fully resolve these contributions. The poor signal-to-noise ratio at this high energy loss (>2100 eV) necessitates the use of long acquisition times, which renders the spectral resolution highly susceptible to instrumental instabilities.

To investigate whether such splittings can be employed to distinguish among the three phases, an alternative approach is to use the Zr $M_{2,3}$ edge. The lower energy loss of this edge makes the experiment less susceptible to instabilities, and since the symmetry of the core level is the same in both cases, the near-edge structure should be essentially identical at the $L_{2,3}$ and $M_{2,3}$ edges. The Zr M edge for each pseudopolymorph is shown in Fig. 6(a). The $M_{2,3}$ edge is superimposed on the tail of the $M_{4,5}$ core excitation, the latter being of little interest for analysis due to the complexity of the electronic transitions which cause it. However, its presence makes subtraction of the background under the $M_{2,3}$ edge difficult. Closer examination of the $M_{2,3}$ edges [Fig. 6(b)] reveals that, although not well resolved, there appear to be multiple contributions to the white lines. To obtain a measure of the splitting at the M_3 component, a linear background was extrapolated under the M_3 edge between 325 and 338 eV. The M_3 edge was fitted using two Gaussian functions and the energy difference between the two functions was taken as the splitting. The procedure was

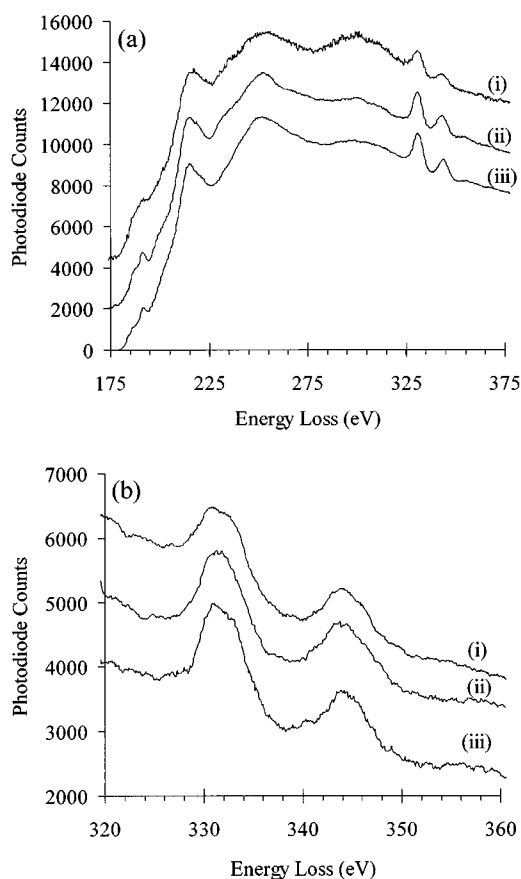


FIG. 6. (a) Zirconium $M_{4,5}$ and $M_{2,3}$ edges for (i) CSZ, (ii) TSZ, and (iii) m -ZrO₂ after background subtraction. (b) Expanded plot showing only the $M_{2,3}$ edges for the same samples.

repeated for a number of spectra and the results are shown in Table III. Within experimental error, there is no significant difference in the splittings measured. The magnitude of the splitting, around 2.4 eV, is similar to that found at the zirconium $L_{2,3}$ edge of m -ZrO₂ by Thromat *et al.*¹⁷ Applying the same analysis method to the M_2 edge yields similar results to those obtained from the M_3 edge, but the statistical errors are greater. The increased error is associated with a number of factors which include the lower signal at the M_2 edge, broadening of the M_2 edge relative to the M_3 edge due to an additional auger decay channel for the core hole, and poorer background fitting due to a more rapidly varying edge shape.

The energy-loss spectra recorded at the oxygen K edge of the three phases are shown in Fig. 7. The edges have been aligned by setting the first maximum in the differentiated spectra to 0 eV. The positions of the peaks in the oxygen K edge relative to this threshold energy are summarized in Table IV. For peaks 1, 4, and 5 the energies given in Table IV and the arrows in Fig. 7 are intended only as a guide to

TABLE III. Splitting energy (eV) of the M_3 edge in ZrO₂.

	Average splitting	Error
Cubic	2.48	0.15
Tetragonal	2.45	0.05
Monoclinic	2.35	0.15

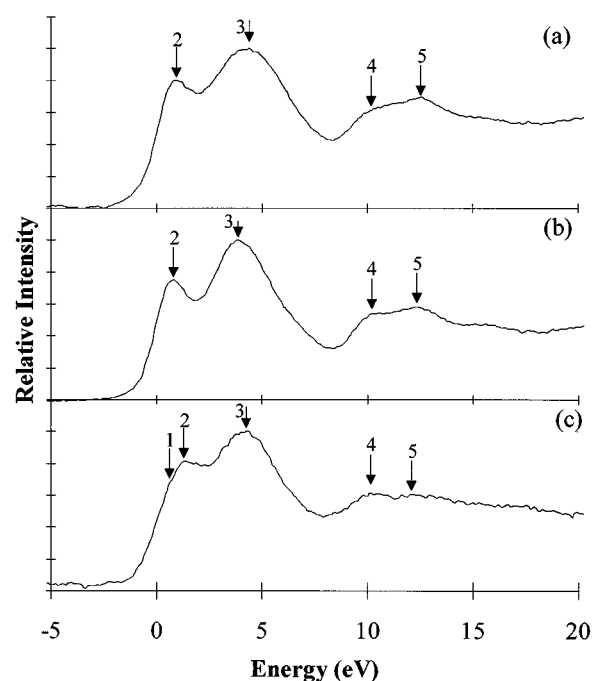


FIG. 7. Plots of the oxygen K -edge spectra for (a) CSZ, (b) TSZ, and (c) m -ZrO₂.

the positions of the peaks. Accurate determination of peak positions for these weak and/or broad features would require additional modeling procedures. While the oxygen K edges from the three samples exhibit the same general shape, there are a number of significant differences. The monoclinic phase can be distinguished from the other phases in two ways; first, by the presence of a low-energy shoulder, peak 1, and second, by the shape of the spectrum 10–15 eV above the threshold. While peak 1 is very weak, it has been observed in a number of spectra and therefore is worthy of note. Although peak 1 might be masked by a small reduction in energy resolution, the spectrum in the higher-energy region is substantially different in shape and intensity to that observed in TSZ and CSZ. The spectral shape in this region is completely reproducible, and thus it is straightforward to identify the monoclinic phase using the oxygen K edge as a fingerprint.

Differences between the cubic and tetragonal phases are present, albeit less obvious. Examination of Fig. 7 reveals

TABLE IV. Peak energies (eV) from the oxygen K -edge spectra of ZrO₂.

Peak	Cubic	Tetragonal	Monoclinic
1	a	a	0.7
2	0.9	0.8	1.4
3	4.	3.8	4.3
4	10.5	10.3	10.2
5	12.5	12.3	12.1
FWHM	7.3	6.5	7.1
Δ	3.5	3.0	2.9

^aPeak absent.

that the spectrum from the cubic phase is broader than that from TSZ in the region of peaks 2 and 3 and in the region of peaks 4 and 5. By considering peaks 2 and 3 as a single band of intensity, the full width at the half maximum (FWHM) of this band (Table IV) can be used to describe the difference more precisely. Similarly, the separation of peaks 2 and 3 (Δ , Table IV) is significantly less in the tetragonal phase, 3 eV, than in the cubic phase, 3.5 eV. Thus, TSZ and CSZ may be differentiated by analysis of the width and separation of the first two peaks at the oxygen K edge.

B. Interpretation of core less excitations: Correlation with electronic structure

The above discussion has established that a ‘‘fingerprint’’ exists for each phase, and that the phases can therefore be distinguished using EELS. The correlation of the experimental spectra with the local coordination environment, via the electronic structure of the materials, will now be addressed. A qualitative view of the electronic structure in terms of molecular orbitals (MO’s) is a reasonable starting point.^{30,31} In the electronic structure of ZrO_2 the lowest unoccupied molecular orbitals (LUMO’s) will be associated with the empty $4d$ orbitals of the Zr atoms. All five d orbitals will have exactly the same energy in a purely atomic view, but this orbital degeneracy is removed in the crystal because of the electrostatic field associated with the oxygen atoms around each Zr atom, i.e., the crystal field.

In its pure high-temperature form, $c\text{-ZrO}_2$ has the fluorite structure and is constructed from regular ZrO_8 polyhedra, in which the oxygen atoms are positioned at the corners of a cube with the Zr atom at the body center. The effect of the cubic crystal field from the oxygen atoms on the Zr d orbitals depends on the symmetry of the orbital. The d_{xy} , d_{xz} , and d_{yz} orbitals point towards the oxygen atoms, while the $d_{x^2-y^2}$ and d_{z^2} orbitals point between the ligands. As a consequence of electron-electron interactions, the latter pair, labeled e_g , are lowered in energy while the former group, labeled t_{2g} , are raised in energy. Thus, two energy levels result, the lower of which is doubly degenerate, and the upper, triply degenerate.³¹ The energy difference between these levels is labeled 10 Dq, the crystal-field splitting parameter, the magnitude of which depends on the strength and symmetry of the crystal field. In general, it can be stated that as the symmetry of the crystal field is reduced, the complexity of the crystal-field splitting will increase and the separation of the energy levels will decrease.

There is some distortion of the crystal field in pure $t\text{-ZrO}_2$, but the ZrO_8 polyhedron remains essentially cubic. Thus, the $e_g\text{-}t_{2g}$ splitting of the Zr d orbitals will be retained, although some broadening, i.e., nondegeneracy, within each group might be expected. In $m\text{-ZrO}_2$ on the other hand, the situation is considerably more complicated since $m\text{-ZrO}_2$ consists of ZrO_7 polyhedra. As there is no center of symmetry in the polyhedra, each d orbital could potentially interact with the crystal field to a different extent. Consequently, it might be expected that all orbital degeneracies would be removed, so that the orbitals may form five distinct energy levels. In fact, recent work suggests that there is a complex (2+1+2) splitting of the d orbitals.²⁶ Finally, as discussed earlier, the stabilized phases can be described as combina-

tions of ZrO_8 and ZrO_7 polyhedra. In TSZ, the lower dopant concentration results in predominance of the ZrO_8 polyhedra and the splitting pattern will be similar to that found in pure $c\text{-ZrO}_2$. The splitting in CSZ will be most realistically described as a weighted average of the splitting patterns found in $c\text{-ZrO}_2$ and $m\text{-ZrO}_2$.

Interpretation of the EELS data within the qualitative MO framework outlined above can now be considered. At the $L_{2,3}$ or $M_{2,3}$ edges, transitions from initial states with p symmetry to final states with s or d symmetry are observed. The $\Delta l = +1$ channel is dominant and, owing to the highly localized nature of the unoccupied d orbitals on the absorbing site, ‘‘white lines’’ occur near the threshold. Prediction of the intensity and relative position of such excitations is complex for d^n ($n \neq 0$) transition elements and must be modeled using atomic multiplet theory.^{27,28} For the case of d^0 systems such as ZrO_2 , on the other hand, the situation is simpler. Two white lines arising from spin-orbit coupling in the initial state are present in the spectrum, and each of these, which represents a $p^6 d^0 \rightarrow p^5 d^1$ transition, is further split by the crystal field. However, the effect of the crystal field must be considered in the context of all possible interatomic interactions,^{27,28} and the result is a complex change in the observed splitting as a function of 10 Dq. Hence, the observed experimental splitting is not, in general, equal to 10 DQ.

The 2.4 eV splitting measured at the M_3 edge of the three pseudopolymorphs is substantially less than the 10 Dq value predicted by trends in the Periodic Table.³² For the reasons given above, this is not unexpected and the magnitude of 10 Dq cannot be directly measured from the Zr core loss spectra. However, the measured splitting should reflect changes in the magnitude of 10 Dq among the three phases. The fact that all three ZrO_2 pseudopolymorphs exhibit very similar experimental splittings (Table II) indicates that either the 10 Dq value is invariant as the local symmetry changes, or, that the $L_{2,3}$ and $M_{2,3}$ edges are relatively insensitive to small changes in 10 Dq. The latter appears to be the more plausible explanation as, based on the qualitative MO description, the substantial symmetry differences among the three pseudopolymorphs will result in significant modifications to the crystal-field splitting.

With respect to the oxygen K edge, only the excitations within 6 eV of the threshold (1,2, and 3) will be considered for the purposes of this discussion. The peaks at higher energy loss must be carefully modeled in order to distinguish direct transitions to unoccupied states from multiple scattering resonances and this is beyond the scope of the current paper. As stated earlier, the initial and final states in EELS are coupled by the dipole selection rule ($\Delta l = \pm 1$). To a first approximation, this means that the oxygen K edge reflects the local p -projected unoccupied density of states. The oxygen configuration would be $1s^2 2s^2 2p^6$ in a purely ionic model, and the $1s \rightarrow 2p$ channel could not contribute to the energy-loss spectrum. However, it is well established that transition-metal oxides can exhibit considerable covalency, which reduces the number of filled states with O $2p$ character.³³ In MO terms, this implies that the unoccupied O $2p$ states will be hybridized with the unoccupied metal $4d$ orbitals. In agreement with earlier studies,³⁴⁻³⁶ the region containing peaks 1, 2, and 3 is therefore attributed to transi-

tions to the O $2p$ weight in states of predominantly zirconium $4d$ character. Since the zirconium $4d$ orbitals will be separated in energy due to the crystal field, it is reasonable to assume that such a splitting will be reflected at the oxygen K edge *via* O $2p$ /Zr $4d$ hybridization. Rigorous analysis of the metal L edges requires the use of atomic multiplet theory, but recent work has shown that such multiplet effects have little influence on the oxygen K edge, even in the presence of substantial hybridization.²⁹ Thus, the starting point for analysis of the oxygen K edges is the assumption that the two main peaks (2,3) are associated with the crystal-field splitting, and that their energy separation, Δ , should be related to the crystal-field parameter, $10 Dq$.

The Δ values obtained (Table IV) are similar in magnitude to those found using other experimental methods,³⁷ and at first glance, the data trend is as predicted for the $10 Dq$ values of the pure zirconia phases. However, in this study it is the stabilized cubic and tetragonal phases rather than the pure zirconia phases that have been investigated, and consequently the correlation of the Δ values with the MO predictions is less obvious. Based on MO arguments the end points of the data trend should be associated with TSZ (ZrO₈ polyhedra) and m -ZrO₂ (ZrO₇ polyhedra), and the Δ value for CSZ (ZrO₈ and ZrO₇) should be somewhere between the values for the former two phases. The experimental measurements are clearly not in agreement with this prediction. It is worth noting that this discrepancy has been largely overlooked in previous XAS studies. The common assumption appears to be that experimental measurements on the monoclinic phase can be directly interpreted in terms of cubic symmetry.³⁸ Given that the crystal-field splittings are highly sensitive to the symmetry of the polyhedra, such an assumption is clearly erroneous.

The correlation between electronic structure and ELNES can also be examined by comparison of the experimental spectra with the results of band-structure calculations for ZrO₂. In Fig. 8, the oxygen K -edge spectra are compared with the partial DOS of oxygen in the three phases of ZrO₂. The partial DOS should also be a symmetry-projected DOS to show the p -like states that are dipole-allowed final states accessible from the oxygen $1s$ core level. However, as in many transition-metal oxides, a symmetry-projected calculation is not essential in this case since the first 5–10 eV of the unoccupied oxygen DOS will be dominated by oxygen $2p$ -derived states.^{29,36} The DOS plots were derived from the band-structure calculations by Zandiehnam *et al.*¹⁸ and have been convoluted with a Lorentzian function (FWHM = 1.0 eV) to simulate the experimental energy resolution. Before comparing the theoretical calculations with the experimental spectra it is worth commenting on the effect of the core hole created during the excitation process on the DOS. The DOS plots used here represent the electronic ground state, and it has been shown by a number of workers that the core hole can result in significant modification of the DOS.^{29,39} However, such effects are, in general, small in transition-metal oxides, having only a minor influence on the DOS, and it is reasonable therefore to directly compare the site and symmetry-projected DOS with the experimental spectra in such cases.²⁹

The comparisons of theory and experiment shown in Fig. 8 suggest that there is reasonable agreement in two cases,

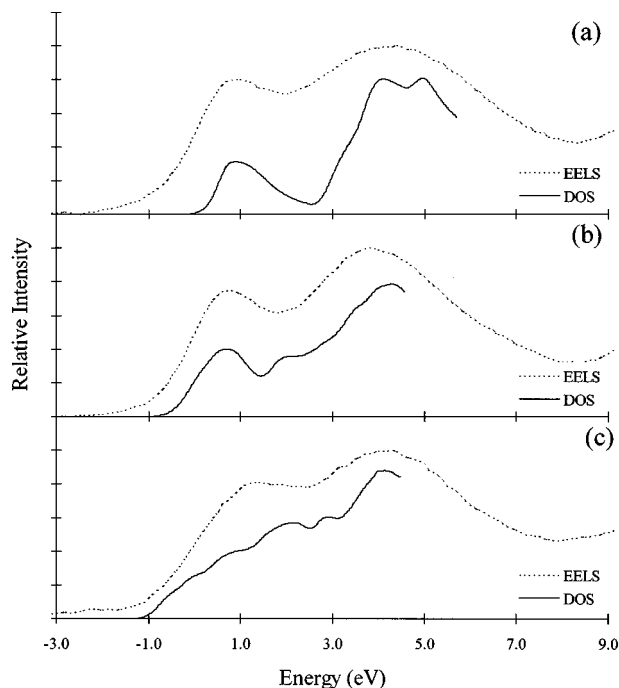


FIG. 8. Comparison of the experimental oxygen K -edge spectra with the calculated oxygen DOS in (a) c -ZrO₂, (b) t -ZrO₂, and (c) m -ZrO₂.

namely cubic and tetragonal, while the correlation between experiment and theory for m -ZrO₂ is extremely poor. The basis for this conclusion is that the DOS for the cubic and tetragonal phases consists of two main bands of intensity, the first weaker than the second, that correspond to the e_g - t_{2g} splitting predicted by MO theory. The experimental spectra reproduce both the position and relative intensity of these bands. Much of fine structure in the DOS plots is absent in the spectra which may be an indication that core-hole effects have some influence on the experimental results. While two peaks are present in the experimental spectrum of m -ZrO₂ the DOS plot does not exhibit a similar splitting, rather the DOS appears to be a single broad asymmetric peak with some fine structure also evident. The nature of the DOS is likely associated with the lack of local symmetry in the m -ZrO₂ structure and the reasons for the poor agreement of this calculation with the experimental spectrum are discussed below.

It is crucial to consider exactly what is being compared in order to understand the agreement as well as the discrepancies between experiment and theory. The DOS calculations are based on vacancy-free room-temperature structures with cubic, tetragonal, and monoclinic unit cells. The comparison of the DOS calculated for t -ZrO₂ with the experimental spectrum of TSZ is valid since both structures are based on ZrO₈ polyhedra and the concentration of O vacancies in TSZ is relatively low. However, it is invalid to compare the CSZ spectrum with the DOS calculated for pure c -ZrO₂, because the former contains significant numbers of ZrO₈, ZrO₇, and YO₈ polyhedra, while the latter contains only perfect ZrO₈ polyhedra. The observed agreement between experiment and theory is therefore purely coincidental. In contrast, the lack of agreement between the experimental spectrum from

m -ZrO₂ and the corresponding DOS is surprising, since it is the pure room-temperature phase that is being investigated in both theory and experiment.

To explain the observations for CSZ and m -ZrO₂ it is necessary to reconsider the FWHM and energy separation, Δ , of peaks 2 and 3 (Table IV) in the experimental spectra.

Examination of these values reveals that the energy difference, Δ , decreases in the sequence CSZ > TSZ > m -ZrO₂. However, the trend in FWHM values is CSZ > m -ZrO₂ > TSZ. One would not intuitively expect a small value of Δ to be associated with a large FWHM, as found for m -ZrO₂, unless there are additional contributions to the edge. Other characteristics of the spectra also indicate that the situation for m -ZrO₂ and CSZ is more complex than in TSZ. For example, analysis of a large number of spectra suggests that peak 1 is present in the oxygen K edge of m -K₂O, it may be present in the spectrum of CSZ, but it is absent in TSZ. In addition, the depth of the minimum between peaks 2 and 3 is greatest for TSZ, and is less pronounced in the other pseudopolymorphs. To account for these observations, as well as the correlation (or lack thereof) between experiment and theory, it is important to consider the initial, as well as the final, state in the energy-loss process, since both are affected by the types of polyhedra present. The symmetry of the polyhedron defines the effect of the crystal field on the outer atomic orbitals and thereby affects the final states. If all of the oxygen atoms that form the polyhedron are not in identical environments then the binding energy of the oxygen $1s$ core levels will vary slightly, leading to multiple initial states.⁴⁰ The initial and final states are then related to the energy-loss spectrum as a product of the resulting joint density of states with the appropriate transition matrix element.

The structure of TSZ contains only ZrO₈ polyhedra and consequently the e_g - t_{2g} splitting is well defined. All of the oxygen atoms in the ZrO₈ polyhedra are identical, and since the dopant concentration is relatively low, it is reasonable to ignore the effect of oxygen vacancies. Thus, there is only one O $1s$ binding energy, i.e., one initial state, and in the TSZ spectrum two relatively narrow peaks associated with final-state effects are observed. In m -ZrO₂, there is also only one type of polyhedron, i.e., ZrO₇. However, the lack of symmetry in this polyhedron results in a complex (2+1+2) splitting in the final state. Such polyhedra also contains two distinct types of oxygen sites, resulting in two different O $1s$ binding energies, and hence two initial states must be considered. The calculated DOS reflects the complexity of

the final state, but gives no insight into the influence of the initial states on the experimental spectrum. It is for this reason that the agreement between experiment and theory is so poor. The situation in CSZ can be described as a weighted average of those found for TSZ and m -ZrO₂, with the additional consideration that there is now a significant number of YO₈ polyhedra. The latter will introduce a third oxygen binding energy into the model, and may require consideration of yttrium-derived defect states. Further experiments are necessary to determine the dopant concentration at which such effects become important. Methods to model the combined effect of binding energy changes and crystal field splittings on the energy-loss spectra are under investigation.

V. CONCLUSIONS

The use of EELS in the investigation of ZrO₂ polymorphs has been evaluated in detail in this study. It has been demonstrated that the Zr $N_{2,3}$ and O K edges exhibit significant differences among the three phases investigated. EELS may therefore be added to the array of techniques used to characterize such systems, with the advantage that in the electron microscope EELS "fingerprints" can be used to differentiate among small grains of cubic, tetragonal, and monoclinic ZrO₂ in the same specimen.

The valence loss spectra collected are in good agreement with data obtained from other techniques, and permit the optical properties of the materials to be characterized with high spatial resolution. The observed ELNES has been qualitatively related to the electronic structure and chemical coordination in each pseudopolymorph within an MO as well as a band-structure framework. Comparisons of theory and experiment reveal the necessity of correctly accounting for oxygen vacancies in structural models if full agreement between experiment and theory is to be achieved. The possibility of using MO theory to model these systems as combinations of polyhedral types is currently being examined.

ACKNOWLEDGMENTS

The author would like to gratefully acknowledge Dr. O. T. Woo, Dr. Y. P. Lin, and Professor G. C. Weatherly for useful discussions. Thanks are due to Dr. O. T. Woo for supplying suitable specimens. The author is grateful to Dr. J. Valach for discussions and assistance with some of the computer programming. The financial support of NSERC (Canada) and the Brockhouse Institute for Materials Research is gratefully acknowledged.

*Present address: Department of Chemistry, University of Glasgow, Glasgow G12 8QQ, Scotland.

¹Y. P. Lin, O. T. Woo, and D. J. Lockwood, *Polycrystalline Thin Films: Structure, Texture, Properties, and Applications*, edited by K. Barmak, M. A. Parker, J. A. Floro, R. Sinclair, and D. A. Smith, MRS Symposia Proceedings No. 343 (Materials Research Society, Pittsburgh, 1994), p. 487.

²O. T. Woo, D. J. Lockwood, Y. P. Lin, and V. F. Urbanic, *Structures and Properties of Interfaces in Ceramics*, edited by D. A. Bonnell, U. Chowdhry, and M. Rühle, MRS Symposia Proceedings No. 357 (Materials Research Society, Pittsburgh, 1995), p. 219.

³A. Wold and D. Kirby, *Solid State Chemistry* (Chapman and Hall, London, 1993).

⁴See, for example, *Zirconia V*, edited by S. P. S. Badwal, M. J. Bannister, and R. H. J. Hannink (Australian Ceramic Society, City, 1992).

⁵R. F. Egerton, *EELS in the Electron Microscope* (Plenum, New York, 1986).

⁶*Transmission Electron Energy-Loss Spectrometry in Materials Science*, edited by M. M. Disko, C. C. Ahn, and B. Fultz (TMS, Warrendale, 1992).

⁷D. K. Smith and H. W. Newkirk, *Acta Crystallogr.* **18**, 983 (1965).

- ⁸C. J. Howard, R. J. Hill, and B. E. Reichert, *Acta. Crystallogr.* **B44**, 116 (1988).
- ⁹P. Li, I. Chen, and J. E. Penner-Hahn, *Phys. Rev. B* **48**, 10 063 (1993).
- ¹⁰G. Teufer, *Acta. Crystallogr.* **15**, 1187 (1962).
- ¹¹M. Morinaga, J. B. Cohen, and J. Faber, *Acta. Crystallogr. Sect. A* **35**, 789 (1979).
- ¹²D. Steele and B. E. F. Fender, *J. Phys. C* **7**, 1 (1974).
- ¹³P. Li, I. Chen, and J. E. Penner-Hahn, *Phys. Rev. B* **48**, 10 074 (1993).
- ¹⁴Ceres Corporation, MA 01 862, USA.
- ¹⁵D. L. Wood and K. Nassau, *Appl. Opt.* **21**, 2978 (1982).
- ¹⁶R. H. French, S. J. Glass, F. S. Ohuchi, Y.-N. Xu, and W. Y. Ching, *Phys. Rev. B* **49**, 5133 (1994).
- ¹⁷N. Thromat, C. Noguera, M. Gautier, F. Jollet, and J. P. Duraud, *Phys. Rev. D* **44**, 7904 (1991).
- ¹⁸F. Zandiehnam, R. A. Murray, and W. Y. Ching, *Physica B* **150**, 19 (1988).
- ¹⁹L. Soriano, M. Abbate, J. Faber, C. Morant, and J. M. Sanz, *Solid State Commun.* **93**, 659 (1995).
- ²⁰N. I. Medvedeva, V. P. Zhukov, M. Ya. Khodos, and V. A. Gubanov, *Phys. Status Solidi B* **160**, 517 (1990).
- ²¹M. Morinaga, H. Adachi, and M. Tsukada, *J. Phys. Chem. Solids* **44**, 301 (1983).
- ²²J. Frandon, B. Brouseau, and F. Pradal, *Phys. Status Solidi B* **98**, 379 (1980).
- ²³R. S. Sokolova, *Sov. J. Appl. Phys.* **41**, 454 (1974).
- ²⁴E. Elizalde, J. M. Sanz, F. Yubero, and L. Galan, *Surf. Interf. Anal.* **16**, 213 (1990).
- ²⁵J. Daniels, C. V. Festenberg, H. Raether, and K. Zeppenfeld, *Springer Tracts in Modern Physics* Vol. 54 (Springer-Verlag, Berlin, 1970), pp. 78–135.
- ²⁶J. P. Crocombette and F. Jollet, *J. Phys.: Condens. Matter* **6**, 8341 (1994).
- ²⁷F. M. F. de Groot, J. C. Fuggle, B. T. Thole, and G. A. Sawatzky, *Phys. Rev. B* **41**, 928 (1990).
- ²⁸G. van der Laan and I. W. Kirkman, *J. Phys.: Condens. Matter* **4**, 4189 (1992).
- ²⁹F. M. F. de Groot, *J. Electron Spectrosc. Relat. Phenom.* **67**, 529 (1994).
- ³⁰F. A. Cotton, *Chemical Applications of Group Theory* (Wiley, New York, 1990).
- ³¹R. G. Burns, *Mineralogical Applications of Crystal Field Theory* (Cambridge University Press, Cambridge, 1970).
- ³²F. A. Cotton and G. Wilkinson, *Advanced Inorganic Chemistry* (Wiley, New York, 1980).
- ³³A. R. West, *Solid State Chemistry and Its Applications* (Wiley, New York, 1984), pp. 290–296.
- ³⁴F. M. F. de Groot, M. Grioni, J. C. Fuggle, J. Ghijsen, G. A. Sawatzky, and H. Petersen, *Phys. Rev. B* **40**, 5715 (1989).
- ³⁵L. A. Grunes, R. D. Leapman, C. N. Wilker, R. Hoffmann, and A. B. Kunz, *Phys. Rev. B* **25**, 7157 (1982).
- ³⁶H. Kurata, E. Lefevre, C. Colliex, and R. Brydson, *Phys. Rev. B* **47**, 13 763 (1993).
- ³⁷L. Soriano, M. Abbate, D. Alders, and J. M. Sanz, *Solid State Commun.* **7**, 551 (1994).
- ³⁸L. Soriano, M. Abbate, J. Faber, C. Morant, and J. M. Sanz, *Solid State Commun.* **93**, 659 (1995).
- ³⁹P. Rez, in *Transmission Electron Energy-Loss Spectrometry in Materials Science*, edited by M. M. Disko, C. C. Ahn, and B. Fultz (TMS, Warrendale, 1992), pp. 107–129.
- ⁴⁰R. Brydson, B. G. Williams, W. Engel, Th. Lindner, M. Muhler, R. Schlogl, E. Zeitler, and J. M. Thomas, *J. Chem. Soc. Faraday Trans. I* **84**, 631 (1988).